PHYSICAL REVIEW A, VOLUME 64, 051803(R)

Generation of subfemtosecond pulses by beating a femtosecond pulse with a Raman coherence adiabatically prepared in solid hydrogen

Fam Le Kien,* Nguyen Hong Shon,† and K. Hakuta
Department of Applied Physics and Chemistry, University of Electro-Communications, Chofu, Tokyo 182-8585, Japan
CREST, Japan Science Technology Corporation, Chofu, Tokyo 182-8585, Japan
(Received 20 March 2001; published 8 October 2001)

We show that the beating of a nanojoule femtosecond pulse with a Raman coherence adiabatically prepared by a pair of millijoule nanosecond pulses in solid hydrogen leads to an efficient generation of a triplet, doublet, or even singlet of subfemtosecond pulses. The energy conversion efficiency of the subfemtosecond pulse generation can be larger than unity due to the transfer of energy from the driving pulses.

DOI: 10.1103/PhysRevA.64.051803 PACS number(s): 42.65.Re, 32.80.Qk, 42.50.Gy, 42.65.Sf

I. INTRODUCTION

The generation of subfemtosecond pulses is of great importance for various applications in science and technology [1]. Different methods have been proposed for the generation of single subfemtosecond pulses and subfemtosecond-pulse trains. One of the promising methods is high harmonic generation with an intense, few-cycle laser pulse in noble gases [2]. A disadvantage of this method is that it produces subfemtosecond pulses with an energy many orders of magnitude lower than that of the pump pulse. Another interesting method is the use of high-order stimulated Raman scattering (SRS) [3–7]. Yoshikawa *et al.* suggested the use of phase-locked Raman lines for short-pulse generation [3]. Harris and Sokolov proposed the use of cw two-color laser beams [4]. Nazarkin *et al.* suggested the use of an impulsive excitation technique [5]. Kalosha and Herrmann proposed the use of subpicosecond pumping followed by external phase compensation [7]. The most important advantage of the SRS techniques is that the energy conversion efficiency is quite high (near-complete conversion can be achieved). A disadvantage is that they lead to trains of many pulses. In addition, the impulsive and short-pulse excitation methods [5,7] require strong pump intensity, for which the Kerr effect and its counteraction on pulse compression are substantial. The shortest length of the pulses generated by these methods is 3 fs, if external phase compensation is not applied.

In this paper we propose a different SRS technique for the subfemtosecond pulse generation: a femtosecond probe pulse beats with a Raman coherence adiabatically prepared by two nanosecond driving pulses in solid hydrogen. This technique combines the advantage of the cw two-color laser pumping [4] in producing large coherences and trains of short pulses and the advantage of the short-pulse excitation [7] in reducing the number of pulses per train. It also utilizes the advantage of solid hydrogen as a Raman medium with high number density, short medium length, small dephasing rate, large coherence length, and negligible phase mismatch [8,9]. In addition, the experiment with a solid can be performed in the vacuum to prevent the chirping of the generated subfemtosecond pulses. Unlike the suggestion of Kalosha and Herrmann [7], the use of nanosecond pumping for the narrow vibrational transition $Q_1(0)$ in solid hydrogen allows us to prepare a substantial coherence at low pump intensity, avoiding the counteraction of the Kerr effect and nonlinear dispersion. Furthermore, without the need for external phase compensation, the probe pulse can be compressed to a triplet, doublet, or even singlet of pulses with a pulse length of 0.5 fs. The energy conversion efficiency of this generation process can be larger than unity due to the transfer of energy from the driving fields to the probe.

II. MODEL AND ANALYSIS

We consider the propagation of a pair of nanosecond pulses, with carrier frequencies ω_0 and ω_{-1}, and a femtosecond pulse, with carrier frequency ω_f, through a Raman medium along the z direction, see Fig. 1. The timing and alignment of these pulses are such that they substantially overlap with each other during the interaction process. The nanosecond pulses are tuned close to the Raman transition $|a\rangle \rightarrow |b\rangle$, but far detuned from the upper electronic states of the molecules. These pulses generate a set of equidistant Raman sidebands collinearly propagating with complex envelopes E_q and carrier frequencies $\omega_q = \omega_0 + q(\omega_{ba} - \delta) = \omega_0 + q\omega_m$ [8,10]. The two-photon detuning δ is the difference between the Raman frequency $\omega_{ba} = \omega_b - \omega_a$ and the modulation fre-

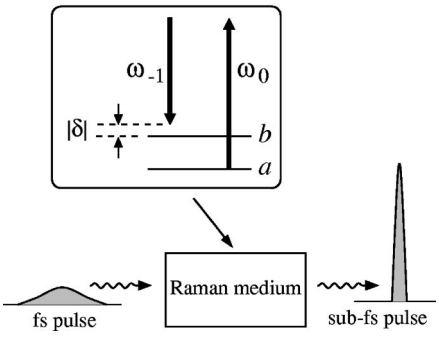

FIG. 1. Principle of the technique: Two nanosecond pulses drive a Raman transition of molecules in a far-off-resonance medium. The beating of a femtosecond probe pulse with the Raman coherence produces a triplet, doublet, or even singlet of subfemtosecond pulses.

*Permanent address: Department of Physics, University of Hanoi, Hanoi, Vietnam.

†Permanent address: Institute for Nuclear Sciences and Techniques, Hanoi, Vietnam.

quency $\omega_m=\omega_0-\omega_{-1}$. We use the local time $\tau=t-z/c$ and work with the density matrix elements $\rho_a=\rho_{aa}^{(S)}$, $\rho_b=\rho_{bb}^{(S)}$, and $\rho=\rho_{ab}^{(S)}e^{-i\omega_m\tau}$, where $\hat{\rho}^{(S)}$ is the medium density matrix in the Schrödinger picture. We distinguish two steps: (1) when the femtosecond pulse is outside the medium and (2) when the femtosecond pulse is inside the medium. In the first step, because only the nanosecond pulses interact with the medium, the slowly varying envelope approximation is valid and, therefore, the envelopes E_q are governed by [4,6]

$$\frac{\partial E_q}{\partial z}=i(N\hbar\omega_q/\epsilon_0 c)[(a_q\rho_a+b_q\rho_b)E_q+d_{q-1}\rho^*E_{q-1}+d_q\rho E_{q+1}]. \quad (1)$$

Here N is the number of molecules per volume, a_q and b_q are the dispersion constants, and d_q are the coupling constants. In this step, the molecular coherence ρ and the population difference $w=\rho_b-\rho_a$ are governed by the equations [4,6]

$$[(\partial/\partial\tau)+(1/T_2)-i\delta\rho]=i(\Omega_a-\Omega_b)\rho+i\Omega_{ab}w,$$

$$(\partial w/\partial\tau)+(w+1)/T_1=2i(\Omega_{ab}^*\rho-\Omega_{ab}\rho^*). \quad (2)$$

Here $\Omega_a=\Sigma_q a_q|E_q|^2/2$ and $\Omega_b=\Sigma_q b_q|E_q|^2/2$ are the Stark shifts, $\Omega_{ab}=\Sigma_q d_q E_q E_{q+1}^*/2$ is the two-photon Rabi frequency, and T_2 and T_1 are the coherence and population decay times.

In the second step, the femtosecond probe pulse beats with the Raman coherence prepared by the nanosecond driving pulses. The medium state does not change substantially during this step. In the paraxial approximation, the wave equation for the probe field E is

$$(\partial E/\partial z)=-(1/2\epsilon_0 c)(\partial P/\partial\tau). \quad (3)$$

Here the polarization P is separated into the contributions from the Raman process P_R, the linear dispersion P_D, and the electronic Kerr effect P_K. The Raman polarization is

$$P_R=2N\hbar E(a_f\rho_a+b_f\rho_b+d_f\rho^*e^{-i\omega_m\tau}+d_f\rho e^{i\omega_m\tau}). \quad (4)$$

The contribution from the linear dispersion is

$$P_D=P_L-2N\hbar a_f E, \quad (5)$$

where the Fourier component of the linear polarization is

$$P_L(z,\omega)=\epsilon_0\chi(\omega)E(z,\omega)=2N\hbar a_\omega E(z,\omega). \quad (6)$$

Here a_ω is the dispersion coefficient a_q evaluated at $\omega_q=\omega$ [4,6]. The polarization produced by the Kerr effect is $P_K=\epsilon_0\chi^{(3)}E^3(t)$.

We extend the analytical treatment of [7] to get insight into our technique, neglecting dispersion, relaxation, and the Kerr effect. According to [4,6], when the two-photon detuning δ and the decay times T_1 and T_2 are large, the medium follows an adiabatic eigenstate with

$$\rho_a=\cos^2\theta, \quad \rho_b=\sin^2\theta, \quad (7)$$

and

$$\rho=e^{i\varphi}\sin\theta\cos\theta, \quad (8)$$

where

$$\tan 2\theta=2|\Omega_{ab}|/(\delta+\Omega_a-\Omega_b) \quad (9)$$

and φ is the phase of Ω_{ab}. For negligible dispersion and limited modulation bandwidth, we have

$$\varphi=\varphi(0)-\kappa z, \quad (10)$$

where

$$\kappa=N\hbar\omega_m u/\epsilon_0 c \quad (11)$$

with

$$u=a_f\rho_a+b_f\rho_b. \quad (12)$$

Then, the polarization reads

$$P=2N\hbar E[u+2d_f\rho_0\sin(\omega_m\tau-\kappa z+\phi)]. \quad (13)$$

Here $\rho_0=|\sin\theta\cos\theta|$ and $\phi=\varphi(0)+(\pi/2)\mathrm{sgn}(\delta)$.

For the treatment of the second step, we neglect the changes of θ in space and time. In this case, the quantities ρ_0, u, and κ are constants. Hence, the solution of Eq. (3) is [7]

$$E(z,\tau)=E_{\mathrm{in}}(s)G, \quad (14)$$

where E_{in} is the input field at $z=0$, the input time s is determined from the equation

$$\tan[(\omega_m s+\phi)/2]=e^{-\alpha z}\tan(\omega_m\eta/2), \quad (15)$$

and the amplitude enhancement factor G is

$$G=\frac{\sin(\omega_m s+\phi)}{\sin\omega_m\eta}=\frac{1}{e^{\alpha z}\cos^2\dfrac{\omega_m\eta}{2}+e^{-\alpha z}\sin^2\dfrac{\omega_m\eta}{2}}. \quad (16)$$

Here we have introduced the retarded time

$$\eta=\tau-z/v+\phi/\omega_m, \quad (17)$$

the effective coupling parameter

$$\alpha=2N\hbar\omega_m d_f\rho_0/\epsilon_0 c, \quad (18)$$

and the effective group velocity

$$v=\omega_m/\kappa. \quad (19)$$

We find that the width compression factor

$$W=\lim_{\Delta s\to 0}\Delta\tau/\Delta s=d\tau/ds \quad (20)$$

is equal to the inverse of the amplitude enhancement factor G:

$$W=1/G. \tag{21}$$

This property leads to the relation

$$\int_{\tau'}^{\tau''} E(z,\tau)d\tau=\int_{s'}^{s''} E_{\rm in}(s)ds, \tag{22}$$

which indicates the conservation of the pulse area.

We introduce the notation

$$\tau_\nu=[(2\nu+1)\pi+\kappa z-\phi]/\omega_m. \tag{23}$$

For $\tau=\tau_n$, where n is integer, we have $\cos(\omega_m\eta/2)=0$ leading to

$$G=1/W=e^{\alpha z}>1. \tag{24}$$

This value indicates a pulse compression in the vicinity of τ_n, with the compression factor $\Gamma=e^{\alpha z}$ [7]. For $\tau=\tau_{n-1/2}$, we have $\sin(\omega_m\eta/2)=0$ leading to

$$G=1/W=e^{-\alpha z}<1. \tag{25}$$

This value indicates a pulse stretch in the vicinity of $\tau_{n-1/2}$.

Compression and stretch, occurring sequentially at τ_n and $\tau_{n-1/2}$, lead to the formation of a train of short pulses with repetition period $T_m=2\pi/\omega_m$ (the Raman period), pulse length T_m/Γ, and maximal frequency and maximal amplitude growing with Γ. Note that τ_n and $\tau_{n-1/2}$ grow with z. In the vicinity of τ_n or $\tau_{n-1/2}$, the input time s is related to the local time τ as $s=s_n+\Gamma(\tau-\tau_n)$ or $s=s_{n-1/2}+(\tau-\tau_{n-1/2})/\Gamma$, respectively, where $s_\nu=[(2\nu+1)\pi-\phi]/\omega_m$. When the duration T of $E_{\rm in}(t)$ is comparable to or smaller than T_m, the structure of the train depends on the relative position of the input-field peak time t_0 with respect to s_n and $s_{n-1/2}$. Namely, if t_0 is in the vicinity of a time s_n (compression time) or $s_{n-1/2}$ (stretch time), the train may have a single pulse or two pulses, respectively. Such a sensitivity is weak when T is much larger than T_m.

With the help of the formula $\sinh x/(\cosh x-\cos t)=1+2\Sigma_{n=1}^{\infty}e^{-nx}\cos nt$ for $x>0$, we can expand the amplitude enhancement factor G into a Fourier series as

$$G=1+2\sum_{n=1}^{\infty}(-1)^n\tanh^n(\alpha z/2)\cos(n\omega_m\eta). \tag{26}$$

The intensity of the nth line in the spectrum of the factor G is proportional to $\tanh^{2n}(\alpha z/2)$. Therefore, it decreases with increasing n and grows with z. This explains the generation of Raman lines during the propagation. When the input pulse width T is comparable to or smaller than T_m, the spectrum of $E_{\rm in}(s)$ with respect to the retarded time η also contains new lines, and hence substantially affects the spectrum of E.

III. NUMERICAL CALCULATIONS

The above analytical treatment does not include group velocity dispersion, which may also contribute to pulse compression [4]. A more rigorous treatment requires numerical calculations. We solve Eqs. (1)–(3) for the parameters of the vibrational transition $Q_1(0)$ in solid hydrogen [8,9]: $\omega_{ba}=4149.7\ \mathrm{cm}^{-1}$, $T_1=40\ \mu$s, $T_2=0.1\ \mu$s, and $N=2.6\times10^{22}\ \mathrm{cm}^{-3}$. We apply the driving pulses at 738 and 1064 nm, both with the same pulse width 10 ns, the same peak intensity 200 MW/cm^2 (4 mJ for the beam size of 500 μm), and the same peak time $\tau=0$. We use the 800-nm probe pulse to beat with the Raman coherence. The constants a_l, b_l, and d_l $(l=q,f,\omega)$ are taken from the calculations for parahydrogen [6]. We use $\chi^{(3)}=7.94\times10^{-23}$ (m/V)^2, deducted from the value for vapor [7], and find that the Kerr effect is negligible in our case. We choose the Raman detuning $\delta=-50$ MHz, at which the conditions for the adiabatic coherence preparation are satisfied and a large value of $|\rho|$ can be achieved [6].

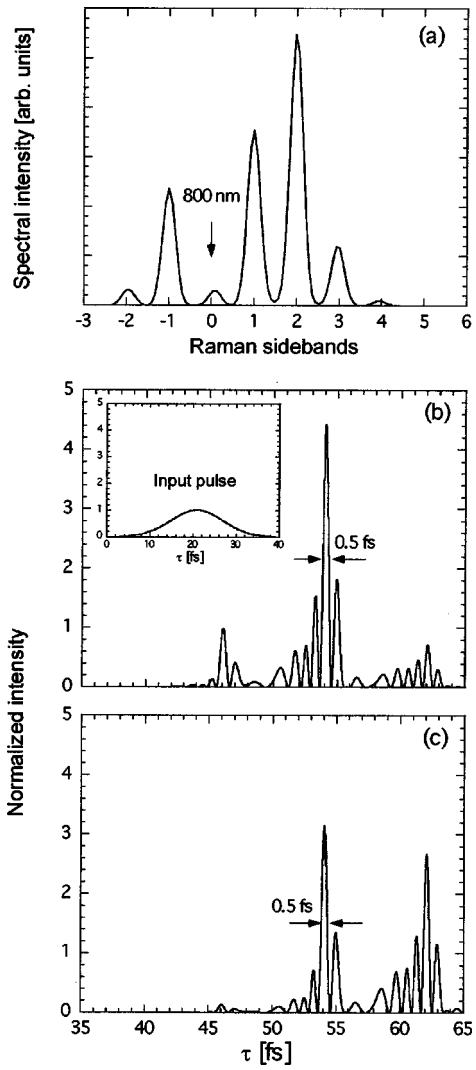

FIG. 2. (a) Spectrum of the probe field. (b) and (c) Temporal profile of the probe field for $t_0=21$ and 25 fs. The parameters are $T=10$ fs, $I_0=200$ MW/cm^2, and $z=125\ \mu$m. The inset in (b) shows the envelope of the input probe pulse. The normalization is the peak intensity of the input probe pulse.

In Fig. 2(a) we plot the spectrum of the probe field at $z=125\ \mu$m for the case where the input pulse width is $T=10$ fs and the input peak intensity is $I_0=200$ MW/cm^2 (2 nJ for the beam size of 300 μm). The spectrum contains

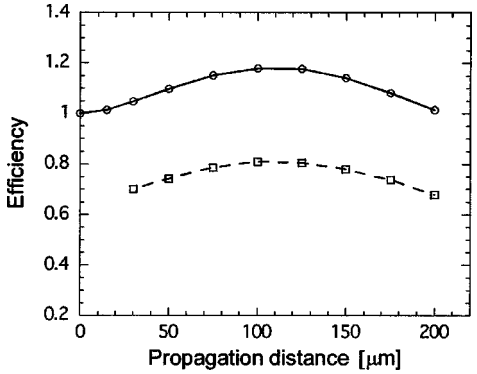

FIG. 3. Energy conversion efficiencies of the pulse triplet (solid line) and the central pulse (dashed line) as functions of the propagation distance. All other parameters are the same as for Fig. 2(b).

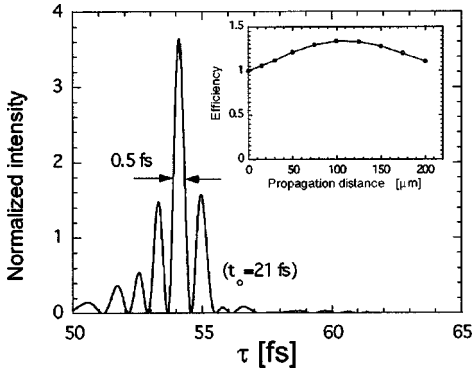

FIG. 4. Single subfemtosecond pulse produced by the beating of a 5-fs probe pulse with the Raman coherence. The input peak intensity is $I_0=1$ GW/cm^2. All other parameters are the same as for Fig. 2(b).

two Stokes lines and four anti-Stoke lines ranging from 2.38 μm to 343 nm. We observe that most of the energy of the central line (800 nm) is converted to its sidebands. The sidebands repeat very well the spectral shape of the input probe pulse, which is quasicontinuous because the input pulse length is short. The spectral intensity is not sensitive to the input-field peak time t_0.

In Figs. 2(b) and 2(c) we plot the temporal profile of the probe field for $t_0=21$ and 25 fs, respectively. All other parameters are the same as for Fig. 2(a). As seen, the shape of the pulse is sensitive to t_0 (with repetition period T_m), in agreement with the analytical results. The temporal profile consists of a triplet, see Fig. 2(b), or a doublet, see Fig. 2(c), of pulses separated by the Raman period $T_m \sim 8$ fs. The central pulse in Fig. 2(b) is compressed by a factor of 20 to 0.5 fs in pulse width, contains a half cycle at the wavelength 525 nm, and has its peak intensity increased by a factor of 4.5.

In Fig. 3 we plot the energy conversion efficiencies of the pulse triplet and the central pulse of Fig. 2(b) against the propagation distance. As seen, the energy conversion efficiency of the pulse triplet is larger than unity. This is a result of the transfer of energy from the driving fields to the probe field via the beating process. The energy conversion efficiency of the central pulse is larger than 50%, quite high as compared to the results of the other techniques. The maximum values of the efficiencies are reached at an optimal length $z \sim 125$ μm, and are 118% for the pulse triplet, and 80% for the central pulse. These maximum efficiencies as well as the general behavior of the pulse triplet do not depend on the intensity of the input probe pulse. When the energy of the input probe pulse is 2 nJ, as used in our calculations, the energies of the pulse triplet and the central pulse are in the range of 1.6–2.4 nJ, very promising for detection and application.

In the above calculations we used the probe pulse with energy of 2 nJ and width of 10 fs because such lasers are commercially available. The use of a shorter probe pulse may allow us to produce a doublet or even singlet of subfemtosecond pulses depending on t_0. In Fig. 4 we illustrate a single subfemtosecond pulse produced by the beating of a 5-fs probe pulse with the Raman coherence. The pulse width is compressed by a factor of 10 to 0.5 fs and the peak intensity is increased by a factor of 3.8. The energy conversion efficiency is larger than unity, see the inset. The shape of the pulse is sensitive to t_0, with repetition period T_m. The value $t_0=21$ fs has been chosen to give the best single subfemtosecond pulse.

IV. CONCLUSIONS

In summary, we have described a different technique for subfemtosecond pulse generation. This technique utilizes the beating of a femtosecond probe pulse with a Raman coherence adiabatically prepared by two nanosecond driving pulses in solid hydrogen. The numerical calculations show that the technique allows us to produce a triplet, doublet, or even singlet of strongly compressed pulses with a high-energy conversion efficiency. To observe the generated subfemtosecond pulses, we should find a way to separate the output of the probe from the pump pulses. This can be done by aligning the pump pulses with a small angle and directing the input probe pulse along the difference of the pump-field wave vectors. The high number density of solid hydrogen allows us to use short medium lengths so that the phase mismatch due to the off-axis pumping is negligible. This issue will be discussed elsewhere [11].

[1] P. Salières *et al.*, Adv. At., Mol., Opt. Phys. **41**, 83 (1999); T. Brabec and F. Krausz, Rev. Mod. Phys. **72**, 545 (2000).
[2] P.B. Corkum *et al.*, Opt. Lett. **19**, 1870 (1994); P. Antoine *et al.* Phys. Rev. Lett. **77**, 1234 (1996); K.J. Schafer and K.C. Kulander, *ibid.* **78**, 638 (1997).
[3] S. Yoshikawa and T. Imasaka, Opt. Commun. **96**, 94 (1993).
[4] S.E. Harris and A.V. Sokolov, Phys. Rev. Lett. **81**, 2894 (1998).
[5] A. Nazarkin *et al.* Phys. Rev. Lett. **83**, 2560 (1999).
[6] Fam Le Kien *et al.*, Phys. Rev. A **60**, 1562 (1999).
[7] V.P. Kalosha and J. Herrmann, Phys. Rev. Lett. **85**, 1226 (2000).
[8] K. Hakuta *et al.*, Phys. Rev. Lett. **79**, 209 (1997); J.Q. Liang *et al.*, *ibid.* **85**, 2474 (2000).
[9] J.Z. Li *et al.*, Phys. Rev. A **58**, R58 (1998); J. Z. Li *et al.* (unpublished).
[10] A.V. Sokolov *et al.*, Phys. Rev. Lett. **85**, 562 (2000).
[11] Nguyen Hong Shon *et al.* (unpublished).